J Appl Electrochem (2012) 42:121–129
DOI 10.1007/s10800-011-0378-9

ORIGINAL PAPER

TiO_2/WO_3 hybrid structures produced through a sacrificial polymer layer technique for pollutant photo- and photoelectrooxidation under ultraviolet and visible light illumination

Maria Ilieva · Aneliya Nakova · Vessela Tsakova

Received: 14 October 2011 / Accepted: 30 December 2011 / Published online: 12 January 2012

Abstract TiO_2/WO_3 hybrid structures were produced on graphite substrates following a three step procedure: (i) electrochemical deposition of WO_3 under potentiostatic conditions, (ii) electrochemical deposition of TiO_2–polyaniline (PANI) composite layers by potentiostatic polymerization of aniline in the presence of TiO_2 nanoparticles, (iii) high temperature (450 °C) treatment for decomposition of the PANI structure. Experiments on the photoelectrochemical response of the composite layers were carried out by cyclic voltammetry and chronoamperommetry in the dark and under illumination by using low power lamps emitting in the visible and UV spectrum ranges. The oxidation of three pollutants—oxalate ions, methanol and malachite green was used to evaluate the photoelectrocatalytic activity of the TiO_2/WO_3 structures. The photocurrents registered for the photooxidation of oxalate were higher than photocurrents measured at hybrid TiO_2/WO_3 electrodes obtained in conventional two-step electrodeposition of WO_3 and subsequently TiO_2 from corresponding salt solutions. The efficiency of the malachite green photodegradation in our experiments was also about two orders of magnitude higher than that obtained in TiO_2/WO_3 structures synthesized in a conventional way. These results are (very probably) due to the proposed synthetic approach involving PANI polymer layer as an immobilizing matrix and the opportunity to disperse homogeneously TiO_2 nanoparticles on the WO_3 surface provided.

M. Ilieva (✉) · A. Nakova · V. Tsakova
Institute of Physical Chemistry, Sofia, Bulgaria
e-mail: milieva@ipc.bas.bg

Keywords Titanium dioxide · Tungsten trioxide · Photoelectrocatalysis · Methanol · Oxalate ions · Malachite green

1 Introduction

Among the materials for photocatalytic degradation of pollutants into less dangerous matter, titanium dioxide remains one of the most promising because of low cost, chemical inertness, non-toxicity and high photostability. Due to the optical band gap, ($E_g = 3.2$ eV, $\lambda = 380$ nm) of the anatase crystalline modification of TiO_2, this material operates under ultraviolet (UV) light irradiation and absorbs less than 5% of the natural solar spectrum. Different approaches have been used in the attempt to narrow this wide band gap and to shift the absorption edge of the TiO_2 toward the visible (VIS) light region [1–4]. Between them is the coupling of TiO_2 as a wide band gap semiconductor with a suitable narrow band gap one, e.g. tungsten trioxide ($E_g = 2.8$ V, $\lambda = 450$ nm). This approach is expected to provide a better charge separation under both UV and VIS light illumination [5].

One of the first comparisons of the photogeneration properties of single component WO_3 and TiO_2 and bi-component TiO_2/WO_3 films were carried out by Shuyanovskaya and Hepel [5, 6]. Thin WO_3 films were deposited by thermal vacuum evaporation and TiO_2 layers were obtained from colloidal dispersion of TiO_2 particles, spread onto conductive glass substrates with and without the WO_3 layer. Increased efficiency of photocurrent generation at band gap excitation was found in the bi-component TiO_2/WO_3 system.

In the recent years various approaches were used to obtain hybrid TiO_2/WO_3 composite films, e.g. powder

sol–gel mixing [7], impregnation and thermal treatment [8–10], magnetron and dc facing targets sputtering [11, 12], pulsed laser deposition [13] and electrosynthesis [14–23]. Electrosythesis was proposed as an alternative route for the production of TiO_2/WO_3 composites offering advantages such as simplicity of equipment, opportunity to control the layer thickness and use various conducting substrates.

Pulsed cathodic electrodeposition was used to obtain composite TiO_2/WO_3 films from two separated or a mixed aqueous bath containing tungsten and titanium precursor species [14–17]. It was found that WO_3 enhances the activity of TiO_2 under UV and VIS irradiation and the TiO_2/WO_3 bi-layer electrodes have improved photoelectrochemical activity in comparison to TiO_2 or WO_3 alone.

Georgieva et al. [18–23] extensively studied the photoelectrochemical activity of TiO_2/WO_3 coatings obtained by potentiostatic electrodeposition from corresponding salt solutions on stainless steel substrates. The TiO_2, WO_3 and TiO_2/WO_3 layers were tested in sulfate, oxalate, 4-chlorphenol, and malachite green (MG) solutions as well as exposed to methanol vapours. It was shown that compared to plain TiO_2 or WO_3 coatings the use of the bi-layer TiO_2/WO_3 structure improves the photooxidation of all tested pollutants under both UV and VIS light illumination.

In a recent study [24] an electrochemical approach for dispersing pre-synthesized TiO_2 nanoparticles into a conducting polymer matrix was suggested based on anodic polymerization of aniline in the presence of the nanoparticles. The obtained TiO_2–polyaniline (PANI) composite layers were found to be photoelectroactive, with photocurrent values depending on the structure of the composite material (single-layered, i.e. PANI–TIO_2, or bi-layered, i.e. PANI + PANI/TiO_2). The first aim of the present work is to extend this approach to the formation of TiO_2/WO_3 hybrid structures by using the conducting polymer as a sacrificial matrix for the immobilization of TiO_2 nanoparticles on pre-deposited WO_3 films. A three step procedure is suggested including: (i) electrodeposition of WO_3, (ii) electrochemical polymerization of aniline in the presence TiO_2, and (iii) high temperature annealing of the TiO_2–PANI/WO_3 composite necessary to decompose the polymer layer.

A further aim of our investigation is to test the WO_3/TiO_2 composite layers with respect to their photoelectrochemical response in the presence of three substances—oxalate anions, methanol and malachite green. Oxalic acid is detected during the mineralization of a large number of organic compounds and is a water pollutant resulting from industrial treatments in the textile industry, metallurgy, etc. [25] Oxalic acid has a strong tendency to adsorb on the TiO_2 surface and was also used as a sacrificial hole scavenger in several photoelectrochemical processes [26]. Methanol is a well known radical scavenger and a non-specific adsorbent to TiO_2/WO_3. It is often chosen as a model, small molecule, electron donating compound to investigate photoelectrochemical oxidation on WO_3/TiO_2 composite layers [12, 27]. MG is a cationic tripheniylmethane dye used in the textile and fish industries [28]. MG has become a highly controversial compound due to the risk it poses to the consumers of treated fish, including its effects on the immune and reproductive systems and its genotoxic and carcinogenic properties [29].

2 Experimental

2.1 TiO_2/WO_3 layer preparation and characterization

All experiments were carried out in a three electrode set-up using platinum plate counter electrode and acid mercury/mercury sulfate reference electrode (MSE) in a compartment with Luggin capillary. The working electrodes were graphite plates with operating surface area of about 0.5 cm^2. Before the electrochemical deposition of the coatings the graphite plates were degreased ultrasonically in 2-propanol for 15 min and dried at 50 °C in air. The backside of the working electrodes was masked by insulating epoxy resin glue. All electrochemical measurements were carried out with a computerized potentiostat Autolab PGSTAT-12 (The Netherlands).

The following three-step procedure was used for the synthesis of TiO_2/WO_3 layers:

(i) electrochemical deposition of WO_3 under potentiostatic conditions ($E = -1.00$ V vs. MSE) in an aqueous solution containing 0.025 M Na_2WO_4 ($Na_2WO_4{\cdot}2H_2O$, Merck, pro analysis), 0.03 M H_2O_2 (30% aqueous solution) and 0.05 M HNO_3 at pH 1.4;

(ii) electrochemical deposition of TiO_2–PANI composite layers by potentiostatic polymerization of aniline ($E = +0.345$ V vs. MSE) in aqueous solution of 0.1 M aniline, 0.5 M H_2SO_4, and 20 g L^{-1} TiO_2 nanoparticles powder (P25, Degussa). This step is carried out under constant magnetic stirring to promote the uptake of TiO_2 particles during the electrodeposition process;

(iii) temperature treatment of the obtained coatings for 1 h at 450 °C to decompose the polymer structure.

Scanning electron micrographs were obtained at JEOL JSM 6390 microscope equipped with energy dispersive spectroscopy (EDS) facility. X-ray diffraction (XRD) was performed with the help of a Philips automatic powder diffractometer (Bragg–Brentano arrangement, fixed slit mode) using CuKα-filtered radiation and scintillation registration.

2.2 Photoelectrochemical characterization of the TiO_2/WO_3 coatings

After synthesis the photoelectrochemical behavior of the TiO_2/WO_3 layers was investigated in a specially designed home-made photoelectrochemical cell with a flat quartz window opposite the working electrode. Aqueous solution of 0.1 M Na_2SO_4 (Merck, pro analysis) at pH 6.5 was used as supporting electrolyte. The photoelectrocatalytic measurements were carried out in the presence of: (i) 0.001–0.055 M $Na_2C_2O_4$, (ii) 0.01–0.2 M methanol, and (iii) 10 ppm MG. Cyclic voltammetric and chronoamperometric measurements on TiO_2/WO_3-coated electrodes were performed in the dark and under illumination. Three consecutive full voltammetric cycles, starting from positive (+0.8 V) to negative potentials (−0.8 V), were carried out in each case in order to achieve steady state response. The specimens were irradiated with UV or VIS lights during the third scan. The volume of the solution in the photoelectrochemical cell was 35 mL.

Radium Ralutec 9 W/78 UVA lamp ($\lambda = 350$–400 nm, $\lambda_{max} = 370$ nm) and Radium Ralutec 9 W/71 VIS light lamp ($\lambda > 400$ nm, $\lambda_{max} = 437$ nm), placed at a distance of 2 cm from the samples, were used for front face electrode illumination. The spectra of the UV and VIS lamps were measured by means of a Bentham M300 monochromator with two diffraction grids and a DH-2 photoelectrical detector (Fig. 1). The average specific power densities, amounting to 11.6 mW cm^{-2} for the VIS lamp and 12.45 mW cm^{-2} for the UV lamp, were determined in air at a distance of 2 cm, using a Scientech Vector S310 power-meter.

A UV–Vis T60 (PG Instruments) spectrophotometer was used to follow the change of the MG concentration upon illumination for different times.

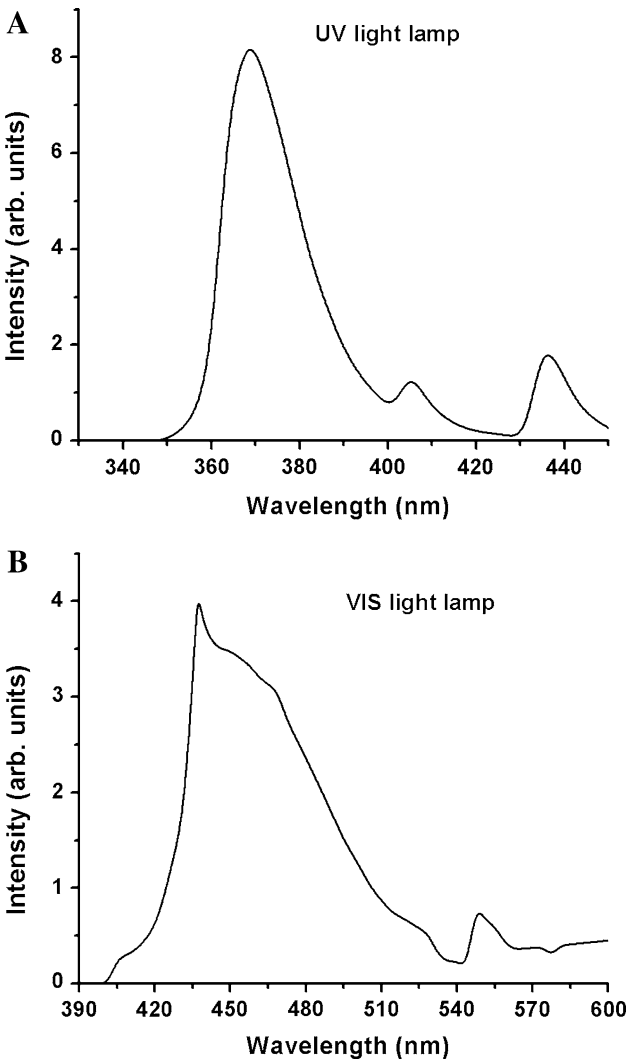

Fig. 1 Spectra of the UV light (**A**) and the visible light (**B**) lamps

3 Results and discussion

3.1 Formation and characterization of TiO_2/WO_3 coatings

Typical chronoamperometric curves for the first (electrosynthesis of WO_3) and second (electrosynthesis of TiO_2–PANI) steps are shown in Fig. 2. In order to optimize the photoelectrochemical response of the TiO_2/WO_3 layers a series of experiments was carried out by varying the duration (from 900 to 5,000 s) of both electrodeposition steps. It was found that the better photoelectrochemical response in supporting electrolyte (see next paragraph) is obtained for layers obtained for 5,000 s of WO_3 deposition (corresponding to 2 mg cm^{-2} WO_3) and 4,000 s of TiO_2–PANI deposition. (Exact quantification of the amount of incorporated TiO_2 is hardly possible in the latter case.)

The typical surface structures of the TiO_2/WO_3 layer obtained after thermal treatment is shown in Fig. 3. The layers consist of large (10–50 μm) cracked WO_3 islands covered with TiO_2 containing agglomerates dispersed over the WO_3 surface. EDS analysis carried out at the TiO_2-modified WO_3 islands (Fig. 3B) shows that the black areas consist of WO_3 and the bright areas of WO_3 and TiO_2. XRD analysis gives evidence for the presence of crystalline monoclinic WO_3 and crystalline anatase TiO_2. It is known that the anatase phase of TiO_2 is more beneficial for high photocurrent generation in comparison with the rutile phase. Cyclic voltammograms of the layers in supporting electrolyte (0.5 M H_2SO_4) carried out after the thermal treatment step do not show the typical fingerprint of the electroactive PANI species and thus confirm the decomposition of the PANI structure during this step.

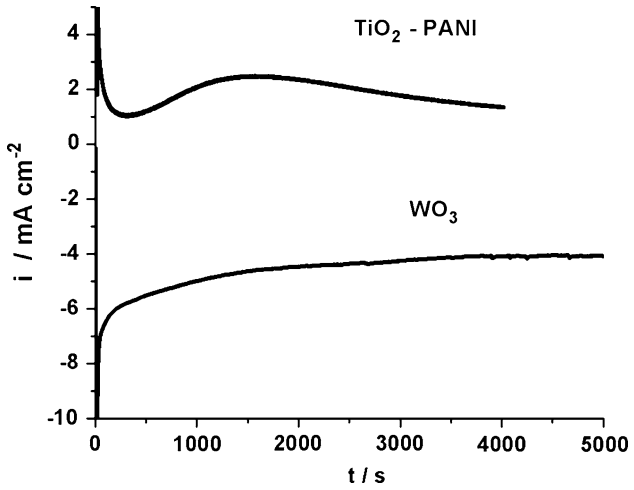

Fig. 2 Current transients measured in the course of WO_3 and TiO_2–PANI electrodeposition

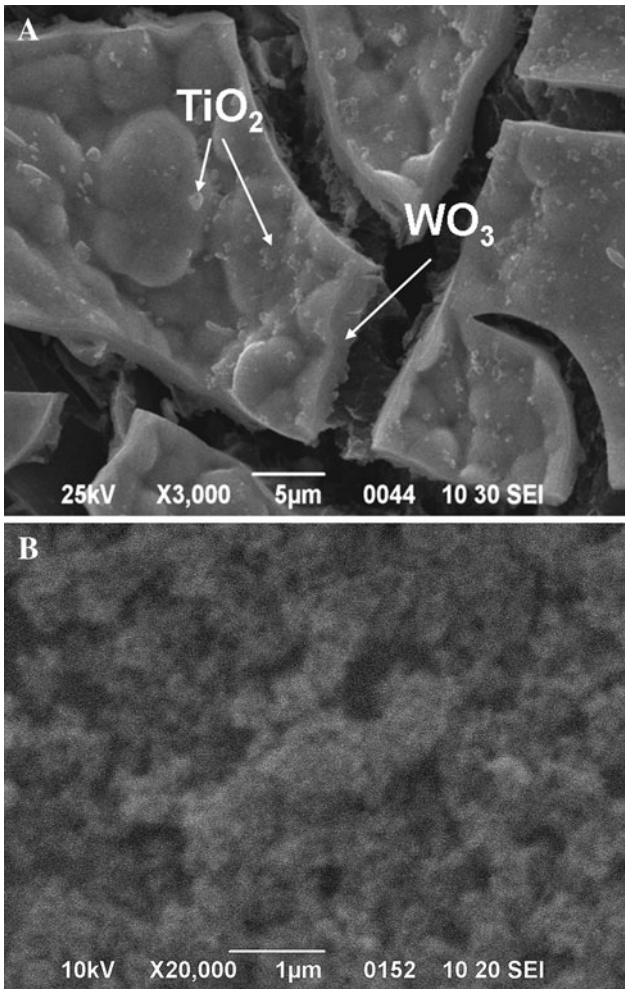

Fig. 3 SEM images at different magnifications of a TiO_2/WO_3 composite after thermal treatment at 450 °C

3.2 Photoelectrochemical response of the TiO_2/WO_3 coatings in supporting electrolyte

Figure 4 shows cyclic voltammetric measurements at TiO_2/WO_3 coated electrodes in the dark and under UV and VIS light illumination. The absence of cathodic currents under illumination is in line with the expected *n*-type semiconductor characteristics of the coatings. After dark current corrections maximum photocurrents are observed at potential $E = +0.7$ V versus MSE (Fig. 4B). Potentiostatic photocurrent response of the composite was measured at this potential using intermittent light (Fig. 5). Significant photocurrent densities (700 µA cm^{-2} for UV light and 350 µA cm^{-2} for VIS light illumination) are detected. These values are higher by factors of about ten than those obtained by conventional two-step electrodeposition of

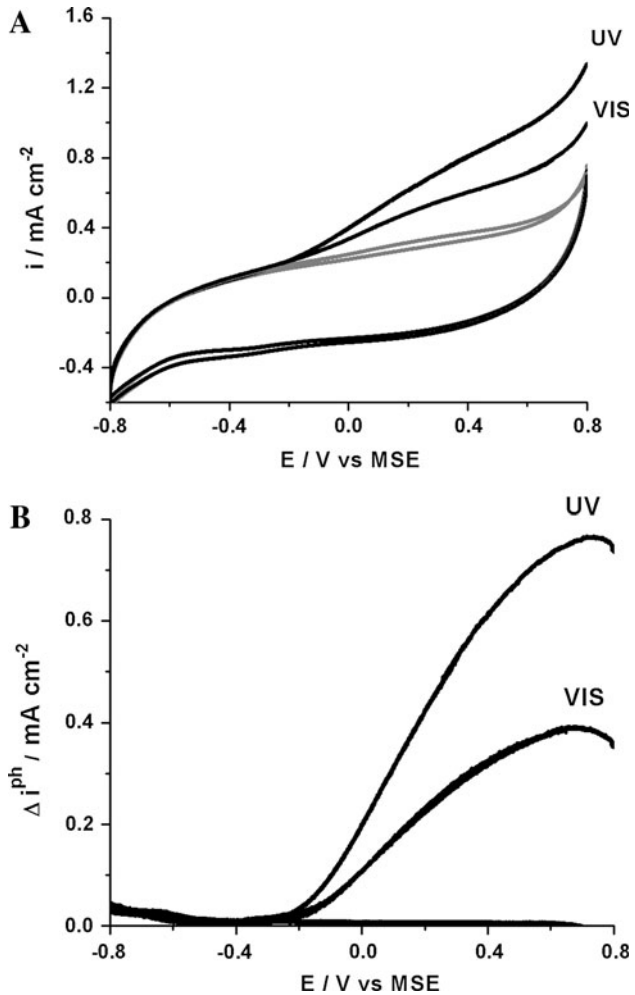

Fig. 4 **A** Cyclic voltammograms measured at a TiO_2/WO_3 composite layer in 0.1 M Na_2SO_4 in the dark (*grey lines*) and under UV and VIS illumination (*black lines*). **B** Voltammograms after dark current subtraction. Scan rate $v = 0.01$ V s^{-1}

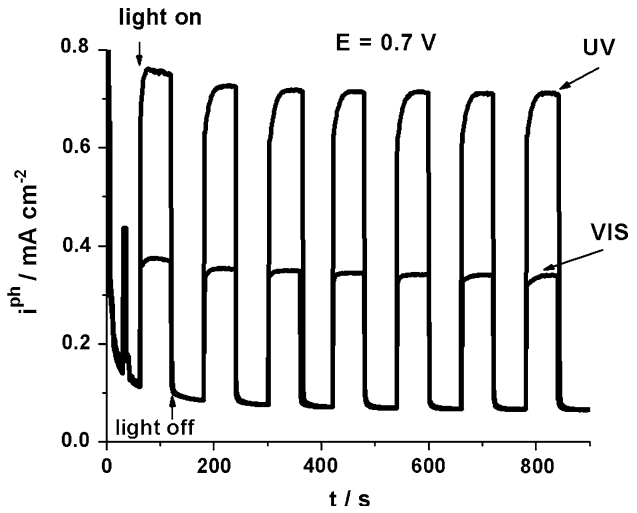

Fig. 5 Potentiostatic photocurrent response at a TiO_2/WO_3 composite layer measured in 0.1 M Na_2SO_4 at a constant potential $E = 0.7$ V versus MSE under UV and VIS intermitted light illumination

WO_3 and TiO_2 from the corresponding salt solutions [18]. This result is very probably due to the opportunity to disperse homogeneously TiO_2 nanoparticles on the WO_3 surface provided by the proposed synthetic approach involving PANI as an immobilizing matrix. It could be suggested that the decomposed sacrificial polymer layer, supports the formation of high surface area TiO_2/WO_3 junctions. The latter are favorable for the efficient separation of the e^-–h^+ pairs generated upon illumination.

3.3 Photoelectrocatalytic activity of TiO_2/WO_3 coatings—oxalate anions

Figure 6 shows cyclic voltammetric curves measured in the presence of oxalate ions in the dark and under both UV and VIS light illumination. The potential window in these measurements was limited to 0.4 V in a way to avoid the electrooxidation of oxalate ions. Marked photoelectrocatalytic currents are observed in both cases together with a significant shift (of about 400 mV) of the photocurrent onset to negative potentials (Fig. 6B). Both the photocurrent increase with respect to the currents measured in the absence of oxalate ions and the shift of the onset potential in negative direction show that oxalate is a better hole scavenger than water. Evidence for direct hole transfer mechanism in the course of oxalate photoelectrooxidation was obtained in the case of anatase TiO_2 electrodes [26] under UV irradiation. By scanning the potential in positive direction within the photocatalytic layer appears a potential gradient, which drives the photogenerated holes and electrons in different directions, inhibits their recombination and stimulates the photocatalytic oxidation of the oxalate ions. Because of the charge separation at the TiO_2/WO_3

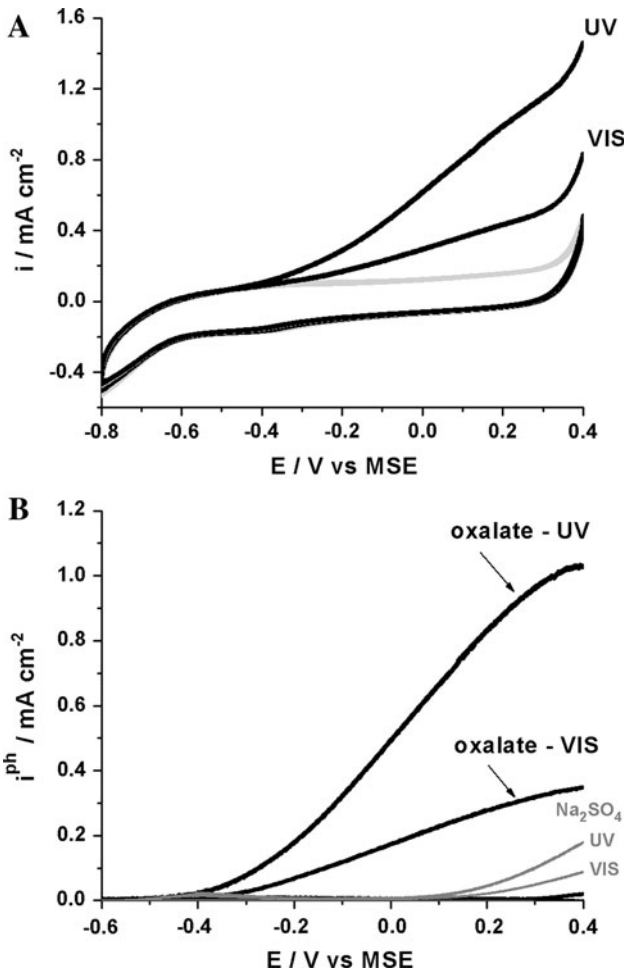

Fig. 6 **A** Cyclic voltammograms measured at a TiO_2/WO_3 composite layer in 0.1 M Na_2SO_4 and 0.025 M $Na_2C_2O_4$ in the dark (*grey lines*) and under UV and VIS illumination (*black lines*). **B** Voltammograms after dark current subtraction**.** Scan rate $v = 0.01$ V s^{-1}

junctions the TiO_2 surface in the bi-component coatings is more positively charged in comparison to the plain TiO_2 surface. This fact leads to a more efficient photooxidation of oxalate through direct interaction with photogenarated holes.

Chronoamperometric measurements carried out at potential $E = 0.3$ V versus MSE (Fig. 7) show rise times of the photocurrents of about 100 s and a stable response thereafter. The plateau region is a result of the consumption of all available photogenerated holes and should depend on the light intensity. A detailed study of the concentration dependence of the saturated oxalate photooxidation currents at fixed potential is shown in Fig. 8. After a narrow concentration range of linear increase of the photocurrents, plateau regions are observed in the 15–50 mM concentration range. The saturation of the photocurrents with increasing oxalate ions concentration should be due to shortage of photogenerated holes under both UV and VIS

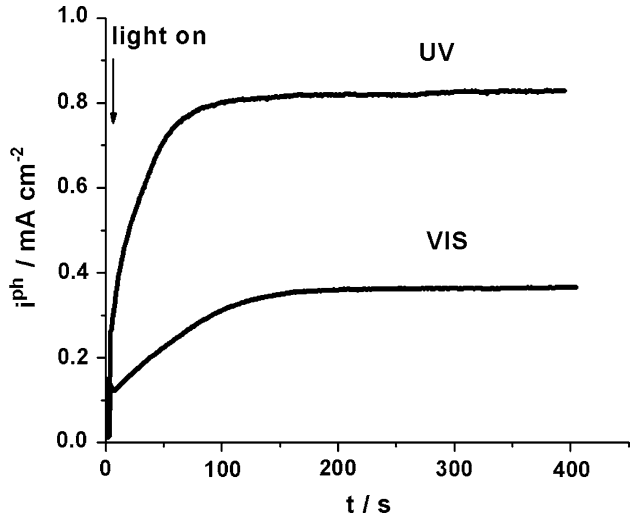

Fig. 7 Photocurrents measured at a TiO_2/WO_3 composite layer in 0.1 M Na_2SO_4 and 0.025 M $Na_2C_2O_4$ solution at a constant potential $E = 0.3$ V versus MSE under UV and VIS light illumination (dark currents are subtracted)

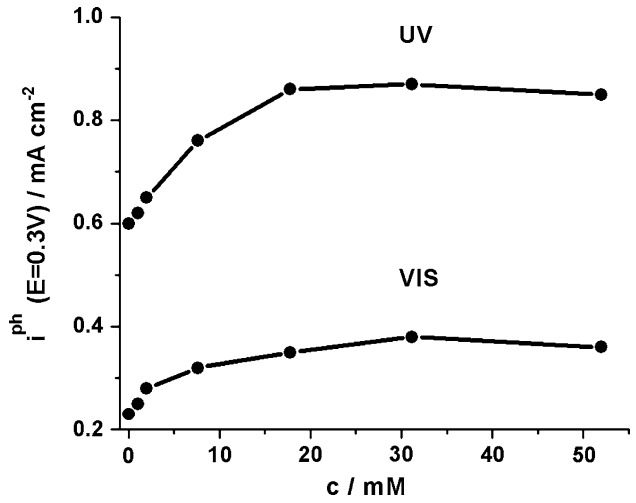

Fig. 8 Concentration dependence of the photocurrent of oxalate oxidation for UV and VIS light illumination from chronoamperometric measurements

light illumination. The higher plateau observed in the UV illumination case is due to the fact that holes become photogenerated not only at the available WO_3 surface (as in the VIS illumination case) but both on WO_3 and TiO_2 free surfaces.

3.4 Photoelectrocatalytic activity of TiO_2/WO_3 composite—methanol

In the presence of methanol, the photocurrents rise again at potentials more negative than in the supporting electrolyte (Fig. 9). The photocurrents obtained after dark current and

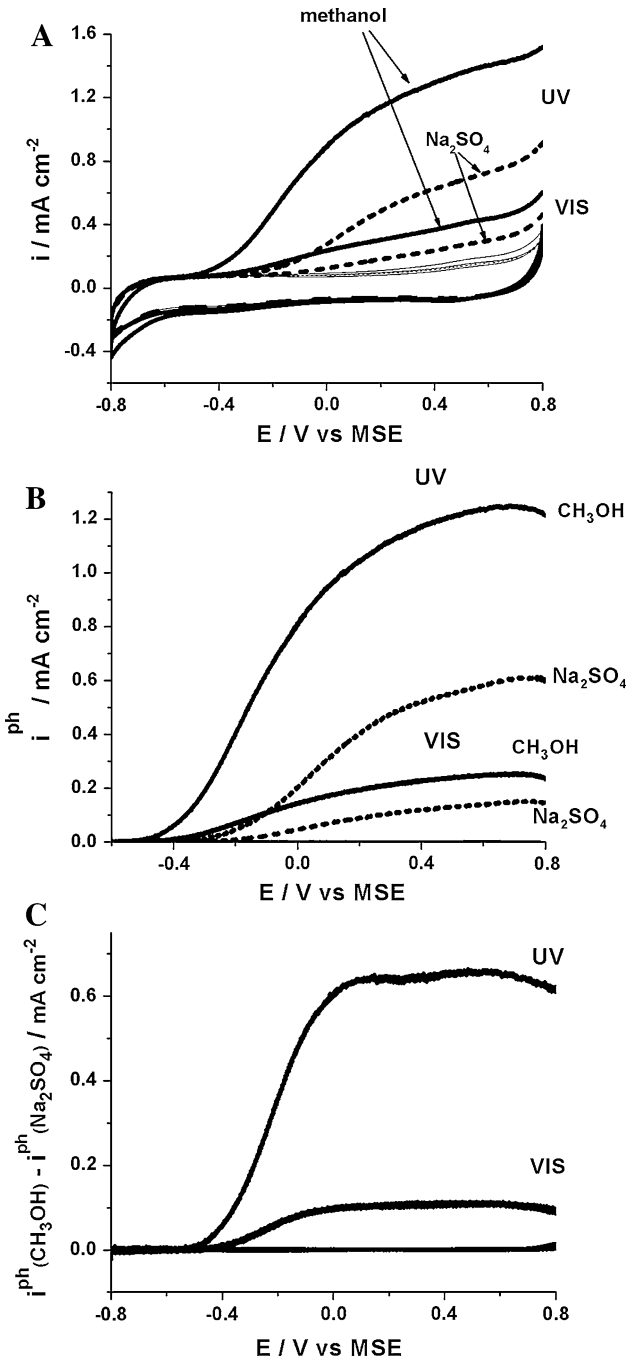

Fig. 9 Cyclic voltammograms measured at a TiO_2/WO_3 composite layer in the absence (*dashed lines*) and in the presence (*black lines*) of 0.05 M CH_3OH in 0.1 M Na_2SO_4 (**A**), after dark currents subtraction (**B**) and after supporting electrolyte current subtraction (**C**). Scan rate $v = 0.01$ V s^{-1}

supporting electrolyte current corrections are shown in Fig. 9B, C. Under illumination the methanol photooxidation current increases linearly with the applied potential before leveling off. The saturated photocurrent may imply that the photogenerated holes are not enough to facilitate the interfacial reaction.

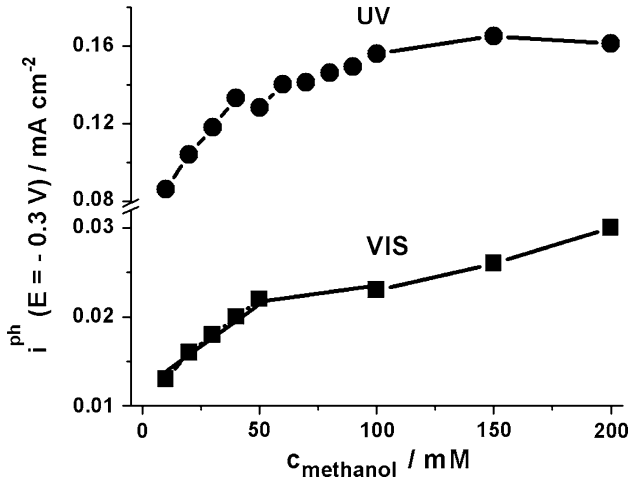

Fig. 10 Concentration dependence of the photooxidation currents of methanol for UV and VIS illumination obtained from voltammetric experiments

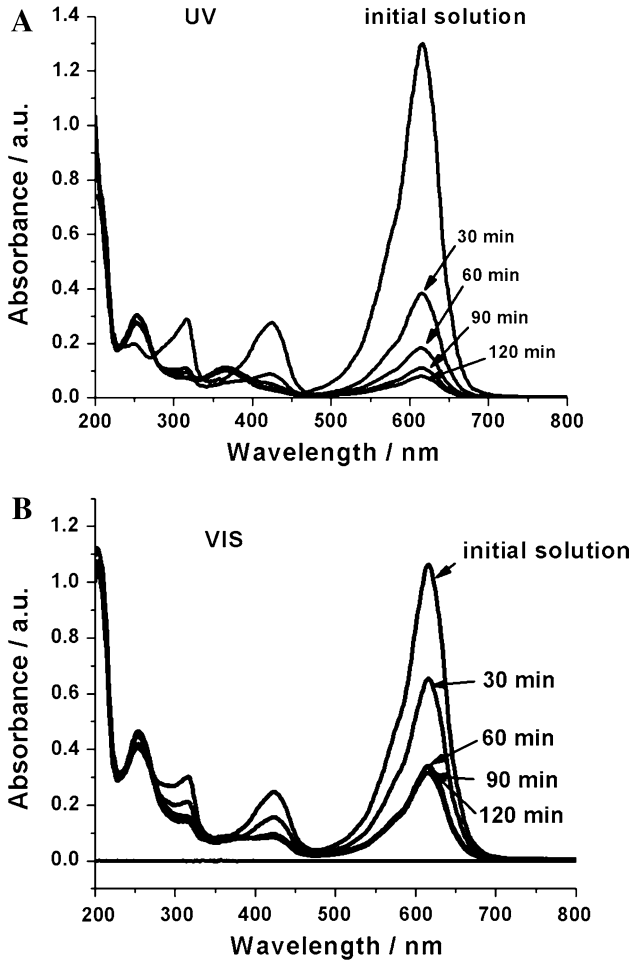

Fig. 11 Absorption spectra measured in a MG solution after different times of exposure at constant potential $E = 0.7$ V versus MSE to **A** UV and **B** VIS light illuminations. The initial concentration of MG is 10 ppm in 0.1 M Na_2SO_4 solution

The investigation of the dependence of the photocurrents (Fig. 10) on the amount of methanol shows a linear region up to 50 mM concentration followed by a plateau region established at higher concentrations. The obtained linear dependence indicates that below 50 mM the overall photocatalytic reaction is under diffusion control. It is suggested [29, 30] that methanol oxidation proceeds mainly though the indirect hole transfer mechanism, i.e. via surface bound hydroxyl radicals. It is generally assumed that the rate of methanol adsorption is lower than the rate at which photogenerated surface bound $OH^{\bullet}$ radicals react with dissolved methanol species [30]. The saturation in the methanol adsorption is the reason for the plateau region of the photocurrent at high methanol concentrations.

3.5 Photoelectrocatalytic activity of TiO_2/WO_3 composite—MG

Finally, the photocatalytic degradation of MG in the presence of the TiO_2/WO_3 composite layer in the solution was studied upon exposure to UV and VIS lights. A solution with 10 ppm MG was irradiated for different times (from 30 to 120 min) by keeping the TiO_2/WO_3 composite-coated electrode at constant potential, $E = 0.7$ V versus MSE. This potential was selected from preliminarily cyclic voltammetric experiments and corresponds to the maximum in the photocurrent response in MG-containing solution. An aliquot of 4 mL was taken out from the reaction mixture after illumination at regular time intervals and absorbance spectra were measured in the wavelength range $\lambda = 200$–800 nm. After the spectrophotometric measurement, the aliquot was brought back in the main solution in order to maintain invariable the initial volume (35 mL) of the solution. Figure 11 shows the absorbance spectra measured after UV and VIS illumination for different times. The absorbance of the visible band at $\lambda = 617$ nm decreases and thereby the concentration of the dye decreases with increasing time of exposure. The absorbance peaks at 425 and 315 nm have also declined, which indicates that the entire conjugated chromophore structure of MG was destroyed [31]. The relative change in the dye concentration (Fig. 12) shows for both UV and VIS lights a rapid decrease (up to 30% for VIS and 14% for UV illumination) within the first 60 min. Further prolongation of the illumination results in almost constant residual dye concentration for the VIS light illumination case and slow (within 120 min) decrease down to 6% from the initial MG concentration for the UV light case.

The comparison on the photodegradation of MG carried out between our system and TiO_2/WO_3 layers produced through conventional electrochemical technique [19] shows the advantage of the approach suggested here. Residual MG concentrations amounting to 15 and 33%

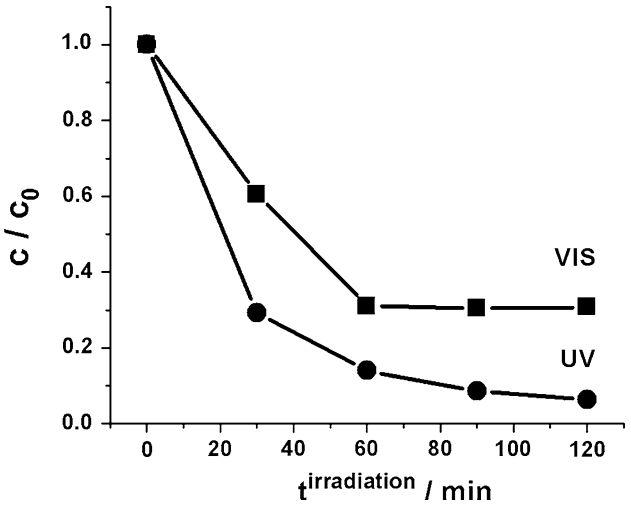

Fig. 12 Relative change of the MG concentration upon exposure to UV and VIS light illumination determined from the absorption maximum at $\lambda = 617$ nm according to Fig. 11

were registered after exposure VIS and UV illuminations, respectively (120 min, 10 ppm initial MG concentration) [19]. These results were obtained using large (30 cm^{-2}) electrodes and large (250 mL) volumes, i.e. by a set-up with volume to surface area ratio of 8.3 mL cm^{-2}. The efficiency of the dye photodegradation under VIS illumination in this case was 0.22 ppm cm^{-2}. In our case, in the same solution and for the same time of photoelectrolysis the residual MG concentration were 6 and 31%, respectively. Although with a more unfavorable volume to surface area ratio (62.5 mL cm^{-2}) the efficiency in our case is 18.8 ppm cm^{-2}, i.e. about two orders of magnitude higher.

4 Conclusions

The proposed electrochemical approach for the synthesis of TiO_2/WO_3 composite layers is based on the immobilization of TiO_2 nanoparticles into a sacrificial conducting polymer material. The immobilization occurs at a pre-deposited electrosynthesized WO_3 layer with thickness that corresponds to the optimal photoelectroactivity of WO_3. The polymer matrix is finally destroyed by temperature treatment thus providing a large area of the TiO_2/WO_3 junctions operating effectively under both UV and VIS light illumination. This specific situation gives rise to markedly higher (by a factor of about 10) photocurrents in supporting electrolyte than those observed by alternatively produced electrochemically deposited TiO_2/WO_3 composite layers.

The comparison of the photocurrents of oxalate oxidation show about an order of magnitude higher values for the TiO_2/WO_3 composites obtained through the sacrificial polymer layer technique in comparison to conventionally produced electrodeposited WO_3 and TiO_2 layers [18]. In the case of UV illumination higher methanol oxidation currents are registered by using the TiO_2/WO_3 composite layers in comparison to TiO_2 thin film electrodes [32].

The observed high efficiency (18.8 ppm cm^{-2}) with respect to MG photodegradation indicates to a hybrid TiO_2/WO_3 material with large surface area that is operating effectively for charge separation.

Acknowledgments The authors are thankful to Prof. N. Vuchkov for the measurements of the UV and VIS lamps spectra. The investigations are carried out within the working program of the project NATO SfP 982835.

References

1. Linsebigler AL, Lu G, Yates JT Jr (1995) Chem Rev 95:735
2. Chatterjee D, Dasgupta S (2005) J Photochem Photobiol C Photochem Rev 6:186
3. Gaya UI, Abdullah AH (2008) J Photochem Photobiol C Photochem Rev 9:1
4. Malato S, Fernandez-Ibanez P, Maldonado MI, Blanco J, Gernjak W (2009) Catal Today 147:1
5. Shuyanovskaya I, Hepel M (1998) J Electrochem Soc 145:3981
6. Shuyanovskaya I, Hepel M (1999) J Electrochem Soc 146:243
7. Song H, Jiang H, Liu X, Meng G (2006) J Photochem Photobiol A Chem 181:421
8. Higashimoto S, Sakiyama M, Azuma M (2006) Thin Solid Films 503:201
9. Higashimoto S, Ushiroda Y, Azuma M (2008) Top Catal 47:148
10. Saepurahman MA, Abdullah FK, Chong J (2010) Hazardous Mater 176:451
11. Takahashi T, Nakabayashi H, Yamada N, Tanabe J (2003) J Vac Sci Technol A 21:1409
12. Biswas S, Hossain MF, Shahjahan M, Takahashi K, Takahashi T (2009) J Vac Sci Technol A 27:880
13. Shinguu H, Bhuiyan MMH, Ikegami T, Ebihara K (2006) Thin Solid Films 506–507:111
14. Chentamarakshan CR, de Tacconi NR, Shiratsuchi R, Rajeshwar Kr (2003) J Electroanal Chem 533:77
15. de Tacconi NR, Chentamarakshan CR, Rajeshwar Kr, Pauporte Th, Lincot D (2003) Electrochem Commun 5:220
16. Somasundaram S, Chentamarakshan CR, de Tacconi NR, Basit NA, Rajeshwar Kr (2006) Electrochem Commun 8:539
17. Somasundaram S, Tacconi N, Chentamarakshan CR, Rajeshwar Kr, de Tacconi NR (2005) J Electroanal Chem 577:167
18. Georgieva J, Armyanov S, Valova E, Poulios I, Sotiropoulos S (2005) J Electroanal Chem 585:35
19. Georgieva J, Armyanov S, Valova E, Poulios I, Sotiropoulos S (2007) Electrochem Commun 9:365
20. Georgieva J, Armyanov S, Valova E, Phillipides N, Poulios I, Sotiropoulos S (2008) J Adv Oxid Technol 11:300
21. Georgieva J, Armyanov S, Poulios I, Sotiropoulos S (2009) Electrochem Commun 11:1643
22. Valova E, Georgieva J, Armyanov S, Sotiropoulos S, Hubin A, Baert K, Raes M (2010) ECS Trans 25:13
23. Georgieva J, Sotiropoulos S, Armyanov S, Phillipides N, Poulios I (2011) J Appl Electrochem 41:173
24. Ilieva M, Ivanov S, Tsakova V (2008) J Appl Electrochem 38:63
25. Addamo M, Augugliaro V, Garcia-Lopez E, Loddo V, Marci G, Palmisano L (2005) Catal Today 107–108:612
26. Waldner G, Gomez R, Neumann-Spallart M (2007) Electrochim Acta 52:2634

27. Jiang D, Zhao H, Jia Z, Cao J, John R (2001) J Photochem Photobiol A Chem 144:197
28. Bojinova AS, Papazova CI, Karadjova IB, Poulios I (2008) Euras J Anal Chem 3:34
29. Jiang D, Zhao H, Zhang S, John R (2006) J Photochem Photobiol A 177:253
30. Villarreal TL, Gomes R, Neumann- Spallart M, Alonsi-Vante N, Salvador P (2004) J Phys Chem B 208:15172
31. Ju YM, Yang SG, Ding YC, Sun C, Zhang AQ, Wang LH (2008) J Phys Chem A 112:11276
32. Li MC, Shen JN (2006) J Solid State Electrochem 10:980